Title

Manipulation of the Ferromagnetism in LaCoO3 Thin Films Through Cation-Stoichiometric Engineering

Journal

Advanced Electronic Materials, 9(5)

ISSN

2199-160X

Authors

Huang, Tongtong
Lyu, Yingjie
Huyan, Huaixun
et al.

Publication Date

2023-05-01

DOI

10.1002/aelm.202201245

ADVANCED ELECTRONIC MATERIALS
Open Access
www.advelectronicmat.de

Manipulation of the Ferromagnetism in $LaCoO_3$ Thin Films Through Cation-Stoichiometric Engineering

*Tongtong Huang, Yingjie Lyu, Huaixun Huyan, Jinyang Ni, Sahar Saremi, Yujia Wang, Xingxu Yan, Di Yi, Qing He, Lane W. Martin, Hongjun Xiang, Xiaoqing Pan, and Pu Yu**

Spin-state transitions are an important research topic in complex oxides with the diverse magnetic states involved. In particular, the low-spin to high-spin transition in $LaCoO_3$ thin films has drawn a wide range of attention due to the emergent ferromagnetic state. Although various mechanisms (e.g., structural distortion, oxygen-vacancy formation, spin-state ordering) have been proposed, an understanding of what really underlies the emergent ferromagnetism remains elusive. Here, the ferromagnetism in $LaCoO_3$ thin films is systematically modulated by varying the oxygen pressure during thin-film growth. Although the samples show dramatic different magnetization, their cobalt valence state and perovskite crystalline structure remain almost unchanged, ruling out the scenarios of both oxygen-vacancy and spin-ordering. This work provides compelling evidence that the tetragonal distortion due to the tensile strain significantly modifies the orbital occupancy, leading to a low-spin to high-spin transition with emergent ferromagnetism, while samples grown at reduced pressure demonstrate a pronounced lattice expansion due to cation-off-stoichiometry, which suppresses the tetragonal distortion and the consequent magnetization. This result not only provides important insight for the understanding of exotic ferromagnetism in $LaCoO_3$ thin films, but also identifies a promising strategy to design electronic states in complex oxides through cation-stoichiometry engineering.

1. Introduction

Transition-metal cations with electronic configurations from d^4 to d^7 can exhibit either high-spin (HS), low-spin (LS) or intermediate-spin (IS) states as a result of competitions between the crystal-field splitting energy (Δ_{CF}), the bandwidth, and the intra-atomic exchange interaction (Δ_{EX}). Lanthanum cobaltite ($LaCoO_3$ or LCO) exhibits a rhombohedral structure with a nonmagnetic insulating ground state, where the LS ($t_{2g}^6e_g^0$) configuration[1] is stabilized since ΔCF is higher than Δ_{EX}. Upon increasing temperature, Δ_{EX} is higher than ΔCF, leading to a spin transition into the HS ($t_{2g}^4e_g^2$) state.[2–4] Interestingly, the IS ($t_{2g}^5e_g^1$) state can also be obtained in distorted octahedra with strong hybridization between the cobalt-e_g orbitals and the p orbitals of the oxygen ligands.[5] More importantly, ferromagnetism has recently been reported in strained LCO thin films,[6,7] in which a pronounced magnetization emerges from

T. Huang, Y. Lyu, Y. Wang, P. Yu
State Key Laboratory of Low Dimensional Quantum Physics and Department of Physics
Tsinghua University
Beijing 100084, P. R. China
E-mail: yupu@mail.tsinghua.edu.cn

H. Huyan, X. Yan, X. Pan
Department of Chemical Engineering and Materials Science
University of California, Irvine
Irvine, CA 92697, USA

J. Ni, H. Xiang
Key Laboratory of Computational Physical Sciences (Ministry of Education)
State Key Laboratory of Surface Physics and Department of Physics
Fudan University
Shanghai 200433, P. R. China

The ORCID identification number(s) for the author(s) of this article can be found under https://doi.org/10.1002/aelm.202201245.

DOI: 10.1002/aelm.202201245

S. Saremi, L. W. Martin
Department of Materials Science and Engineering
University of California, Berkeley
Berkeley, CA 94720, USA

S. Saremi, L. W. Martin
Materials Sciences Division
Lawrence Berkeley National Laboratory
Berkeley, CA 94720, USA

D. Yi
State Key Laboratory of New Ceramics and Fine Processing
School of Materials Science and Engineering
Tsinghua University
Beijing 100084, P. R. China

Q. He
Department of Physics
Durham University
Durham DH13LE, UK

X. Pan
Department of Physics and Astronomy, and Irvine Materials Research Institute (IMRI)
University of California, Irvine
Irvine, CA 92697, USA

the paramagnetic state. Due to its intrinsic ferromagnetic insulating state, LCO thin films obtain considerable interest over the last decades.

To account for the emergent ferromagnetic state in strained LCO thin films, various mechanisms including strain-induced lattice distortion,[8–13] oxygen vacancy formation,[14–17] orbital ordering,[18] spin ordering,[19,20] have been proposed and debated over the last couple decades. Despite the extensive research efforts, a consensus regarding the underlying mechanism has not been obtained. For instance, the presence and role of oxygen vacancy and spin-state ordering have been heavily debated with contradicting results reported. In some studies, a periodic superstructure with dark stripes perpendicular or parallel to the film–substrate interface was observed in atomically resolved images of strained LCO thin films, which have been attributed to the alternating spin ordering of HS and LS Co^{3+} ions.[19,20] While in other studies, these stripe-like structures were assigned as ordered oxygen-vacancies,[13,21] which leads to electron doping with the formation of HS Co^{2+} ($t_{2g}^5e_g^2$) and results in a ferromagnetic insulating state through super-exchange-like interactions. These studies trigger a series of immediate questions to address. Whether oxygen vacancies (or stripe structures) are indeed formed in LCO thin films? Whether the oxygen vacancies (and the subsequent HS Co^{2+}) are beneficial or deleterious for the magnetization? And, what forms the essential tuning knob for the magnetization state in LCO thin films.

Here, we carry out a comprehensive study of the magnetic properties of tensile-strained LCO thin films grown at a series of controlled oxygen pressures. We observe a close correlation between the tetragonal distortion with the ferromagnetism wherein films grown at reduced oxygen pressures show smaller tetragonal distortion (closer to cubic with lattice expansion) and smaller magnetization. The subsequent studies of the electronic (valence) state and atomic crystalline structure of the thin films rule out the contribution of oxygen vacancies as the films exhibit a robust Co^{3+} valence state and stripe features are absent for all strained LCO thin films. Instead, compositional analysis suggests a systematic evolution of cation non-stoichiometry along with the decrease of growth pressure, which leads to a distinct lattice expansion along the film normal, and consequently a suppression of the LS-to-HS spin transition due to a structurally driven orbital reconstruction. This study not only provides important insight for the intrinsic mechanism of ferromagnetism in strained LCO thin films, but also suggests a fertile ground to manipulate the electronic and magnetic states in complex oxide through cation-stoichiometric engineering.

2. Results and Discussion

Epitaxial, high-quality $LaCoO_3$ thin films with the thickness of ≈30 nm were grown on (001) orientated $(LaAlO_3)_{0.3}$-$(SrAl_{0.5}Ta_{0.5}O_3)_{0.7}$ (LSAT, a = 3.871 Å) substrates via pulsed-laser

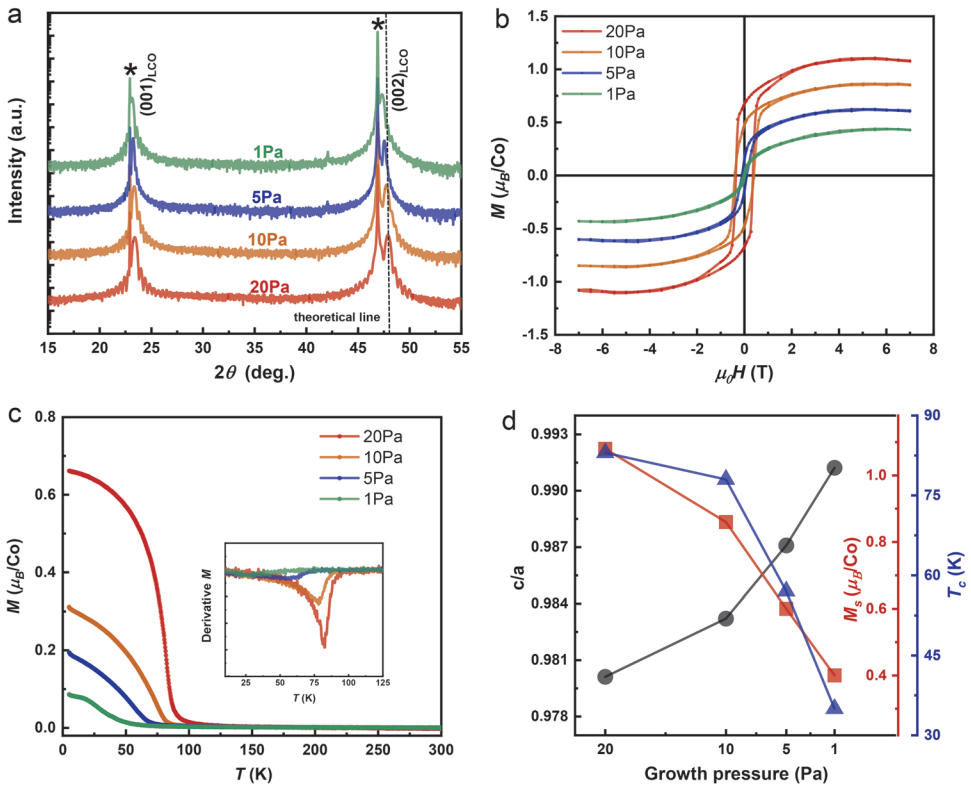

Figure 1. Correlation between structural deformation and magnetization in strained LCO thin films. a) X-ray diffraction (XRD) 2θ–ω scans of LCO thin films grown on LSAT substrates under various oxygen partial pressures. The dashed line indicates the peak position for stoichiometric sample. b) In-plane magnetic hysteresis loops (M–H) of LCO thin films. c) Comparison of temperature-dependent in-plane magnetization (M–T curves) for LCO thin films grown at various pressures. The magnetic field of 1000 Oe was used for the measurements. d) Summary of c/a ratio (black dotted line), saturated magnetization (red dotted line), and Curie-temperature (blue dotted line) as functions of growth partial pressures.

deposition at various oxygen partial pressures of 1, 5, 10, and 20 Pa (see supplementary information for details). X-ray diffraction-based 2θ–ω scans (**Figure 1**a) reveal that all LCO thin films exhibit fully epitaxial, single-phase nature with a high crystalline quality as distinguished by the distinct Laue oscillations around the diffraction peaks. Furthermore, upon decreasing the growth pressure (from 20 Pa to 1 Pa), the out-of-plane lattice constants (c) increases from 3.79 Å to 3.84 Å, leading to a suppressed tetragonal distortion. Reciprocal space mapping studies (Figure S1, Supporting Information) confirm that all films are coherently strained to the substrates, and the lattice is expanded (by 1.3%) along the out-of-plane direction, consistent with the previous studies.[13] Symmetric satellite peaks near the central diffraction peak are identified in all films, which are related to the ferroelastic twinning domain structure in the LCO thin films.[22–24] With a Poisson ratio of ≈0.33 for LCO, we calculated the theoretical 2θ position of LCO film coherently grown on LSAT as labeled by the dot line in Figure 1a, which is close with the value of film grown at 20 Pa.

To explore the evolution of the ferromagnetic properties of the thin films grown at different pressures, we measured both the magnetic hysteresis loops (M–H loops, Figure 1b) and temperature-dependent magnetization (M–T curves, Figure 1c) for a series of samples. All films exhibit well-defined M–H hysteresis loops, while the saturated magnetization (M_S) decreases from ≈1.1 to ≈0.4 μ_B/Co as the growth pressure is reduced from 20 Pa to 1 Pa which is consistent with the a previous study of LCO thin films grown at various pressures.[25] Similarly, the M–T curves reveal a moderate decrease of the ferromagnetic transition temperature (T_C) from 83 to 35 K, as the growth pressure is decreased from 20 Pa to 1 Pa. Figure 1d summarizes the evolution of the tetragonal distortion (c/a), the T_C, and the M_S as a function of the growth pressure. The comparison reveals that the magnetic properties are strongly correlated with the tetragonal distortion, in which LCO thin films grown at lower pressure show a c/a ratio close to one, with both suppressed magnetization and ordering temperature.

Conventionally, the oxide sample grown at reduced pressure would involve the formation of oxygen vacancies, which could result in a chemical expansion. To assess this scenario, we investigated the valence state of the cobalt cations using X-ray absorption spectra (XAS) measurements (Experimental Section), with a bulk-sensitive technique of luminescence yield (FY) mode. As shown in **Figure 2**a, the cobalt L-edge XAS spectra for all LCO films (top panel) exhibit almost identical $L3$ peak position (≈779.05 eV), which strongly suggests a robust Co^{3+} valence state in all films. For comparison, three reference spectra[26] of CoO, Sr_2CoO_3Cl, and $EuCoO_3$ (bottom panel) are also plotted in Figure 2b, corresponding to the absorption of HS Co^{2+}, HS Co^{3+}, and LS Co^{3+}, respectively. We note that these spectra can be employed as effective "fingerprints" to trace both the valence state and spin state of the cobalt cations. Specially, the absorption spectra of HS Co^{2+} have a distinct shift toward lower energy as compared with the other reference spectra from Co^{3+}; furthermore, we notice that its line-shape is also distinct from the XAS spectra (Figure 2a) observed in this work. Interestingly, although the XAS of both HS- and LS-Co^{3+} cations show almost identical peak positions, they have notably different features at the shoulder (Figure 2b), labeled as A (≈777.1 eV) and

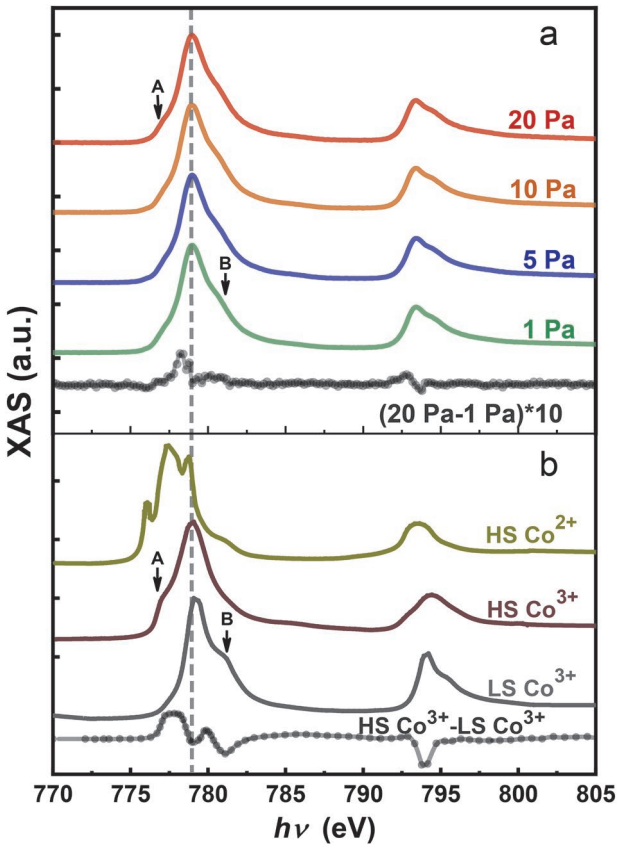

Figure 2. Evolution of Co spin states in LCO thin films. a) Soft X-ray Co-L edges absorption spectra of LCO thin films grown under various oxygen pressures. The spectra were taken with the bulk-sensitive fluorescence-yield mode. b) Reference spectra of high-spin (HS) Co^{2+}, HS Co^{3+} and low-spin (LS) Co^{3+}states. The data were replotted from previous work,[31] taken at CoO, Sr_2CoO_3Cl, and $EuCoO_3$, respectively.

B (≈780.8 eV) for HS and LS Co^{3+}, respectively. Since both A and B peaks appear in the XAS spectra shown in Figure 2a, we deduce that all LCO thin films possess both HS and LS Co^{3+}. With these as a guide, we can assign the slightly different pre-peak features of our LCO thin films to the different HS- and LS-concentrations for Co^{3+} ions. To visualize the different spin states among different samples, we subtract the XAS spectra between the samples grown at 20 Pa and 1 Pa (black curve in Figure 2a), which nicely resemble the different spectra between HS and LS Co^{3+} as shown in the bottom of Figure 2b. This indicates the films grown at lower pressures have lower fractions of the HS state. Therefore, we attribute the modified magnetization observed in thin films grown at various oxygen pressure to the different concentrations of HS Co^{3+} ions.

To probe whether the HS- and LS-Co^{3+} cations form stripe features, we carried out atomic-resolution STEM measurements on the LCO films grown at various pressures. It is important to note that before the STEM sample preparation, we sputtered a thin layer of iridium to protect the samples from beam damage during the focused ion beam (FIB) sample preparation. High-angle annular dark-field (HAADF) cross-sectional images along both the $[100]_{pc}$ and $[110]_{pc}$ zone axes of the LCO grown at 1 Pa (**Figure 3**a,b) and 20 Pa (Figure S3, Supporting

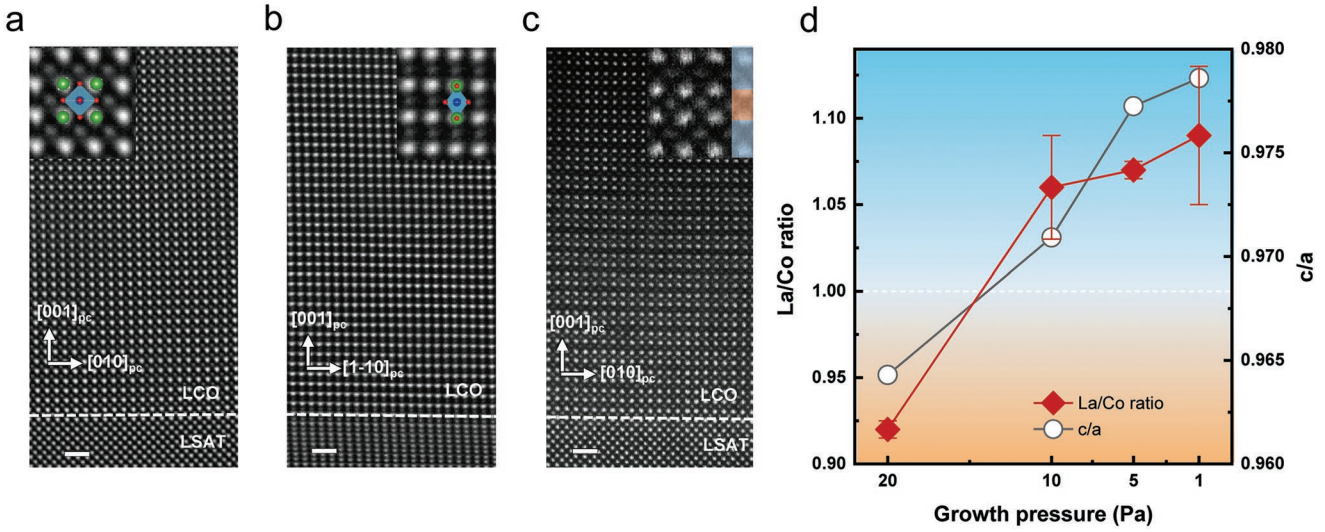

Figure 3. Intrinsic and extrinsic structural transformation in LCO thin films grown at various oxygen pressures. a,b) Cross-sectional HAADF-STEM images on $[100]_{pc}$ (a) and $[110]_{pc}$ (b) zone axis of capped-LCO thin films. The samples were grown at reduced oxygen pressure of 1 Pa. c) STEM images on $[100]_{pc}$ zone axis of uncapped-LCO thin film. The sample was grown at 20 Pa oxygen pressure. The pseudocubic (pc) notation is used for these images. The insets in (a,b) show enlarged HAADF-STEM images overlapping with corresponding perovskite structures, while the inset in (c) contains the enlarged HAADF-STEM images with the modified lattice spacings due to the oxygen vacancy formation. All scale-bars: 2 nm. d) Correlation between the cation-stoichiometric ratio with the lattice expansion.

Information) illustrate that both films, regardless of the growth pressure and projected directions, exhibit nearly ideal perovskite structure without any visible defects and stripe features. Interestingly, in samples without the iridium capping layer, we observed striking stripe features (Figure 3c and Figure S3, Supporting Information). These results suggest that the stripe features are not intrinsic features of the LCO thin films, but are instead attributed to the formation of oxygen vacancies during the sample preparation.[27]

Since the thin films show undetectable oxygen vacancies regardless of the growth pressure, as evidenced by the absent Co^{2+} XAS feature (Figure 2) as well as the excellent perovskite feature in the STEM images (Figure 3), we can safely rule out the oxygen-vacancy formation as the cause for the observed lattice expansion for samples grown at lower pressure. Alternatively, it is known that the change of oxygen pressure can also influence the cation composition of thin films.[28,29] To probe quantitatively the chemical composition of all LCO thin films, we carried out Rutherford backscattering spectrometry (RBS) studies. Because LSAT contributes a strong lanthanum signal overlapping with the signal from the LCO thin films, we completed the RBS studies on the sibling films grown on (001) oriented $SrTiO_3$ substrates with identical growth conditions, in which a consistent change of magnetization with varying oxygen growth pressure was observed (Figure S2, Supporting Information). As shown in Figure S4, Supporting Information, the cation concentration ratios of La/Co are estimated as 0.92 (±0.01), 1.06 (±0.03), 1.07 (±0.01), and 1.09 (±0.04) for LCO grown at the oxygen pressures of 20, 10, 5, and 1 Pa, respectively. In turn, this evolution of cation stoichiometry can be directly correlated with the observed lattice expansion (Figure 3d), as a recent study of $SrTiO_3$ reveals that the Sr/Ti off-stoichiometry could lead to the lattice expansion up to 3.8%.[30]

We now try to address why the films grown at lower oxygen pressure possess higher lanthanum content. It is important to note that although pulsed-laser deposition has been historically considered as a technique with an excellent congruent transfer of target species during ablation, this commonly conveyed knowledge has faced great challenges. The film composition was greatly influenced by the atomic mass of the ejected species, the laser fluence (or energy density), growth pressure, etc.[28,29,31–33] Specifically, although the control of oxygen background pressure has been widely taken as an effective approach to control the oxygen content in oxides, it can also influence the cation composition due to the change of kinetic energy for the plasma species. For instance, it has been shown that the growth of $La_{1-x}Sr_xMnO_3$ at intermediate pressures results in manganese cation deficiency due to the enhanced scattering events with the background molecules for the lighter element.[28] Similarly, in the current study, the LCO grown at a lower oxygen pressure (≈1 Pa) can result in cation off-stoichiometry with Co deficiency, as the scattering effect dominates for a near free-expanded plasma. While with higher oxygen pressure (≈20 Pa), the plasma plume forms a well-defined shape, in which the process shows an excellent congruent transfer of target species with fully optimized growth conditions (laser energy density, substrate temperature, substate-target distance, etc.).

Furthermore, we note that the La-rich phase would lead to the formation of antisite defects, due to the facts that the lattice remains a perovskite structure and the Co valence state show a robust Co^{3+}. With the antisite defects, the magnetic interaction between Co ions would be naturally suppressed, however the small content (≈7%) of antisite defects could not account for the dramatically change (≈70%) of magnetization. On the other hand, because the La ion has much larger radius than the Co ion, the antisite defect would lead to a pronounced lattice

ADVANCED ELECTRONIC MATERIALS
Open Access
www.advelectronicmat.de

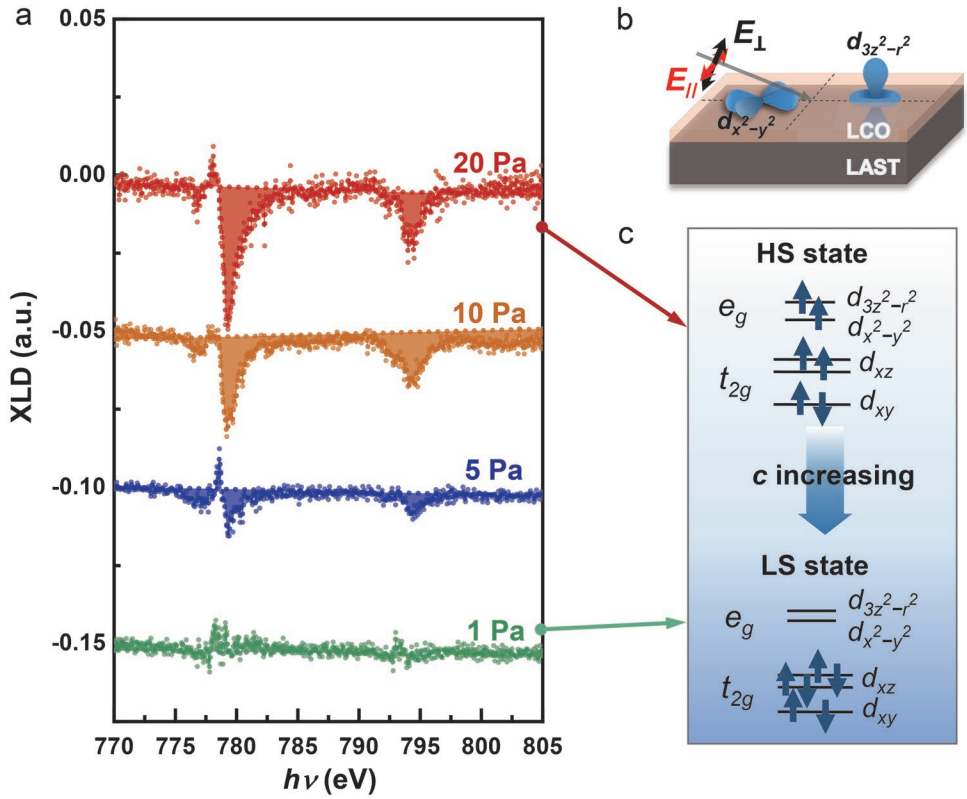

Figure 4. Spin-state transition as evidenced by orbital reconstruction of Co ions. a) X-ray linear dichroism (XLD) at Co^{3+} *L*-edges of LCO thin films grown under various oxygen pressures. b) Experimental scattering geometry during the XLD measurements. The XLD spectra are calculated by the difference between the sXAS of two linearly polarized beams, *E*// and *E*⊥. c) Schematic orbital occupancy of Co^{3+} ($3d^6$) ions at different spin states.

expansion as experimentally observed, which we believe is the dominate factor for the suppressed magnetization.

To further elaborate the evolution of the spin-state with the lattice expansion (i.e., tetragonal distortion), we experimentally probed the orbital occupancy of the Co^{3+} cations through X-ray linear dichroism (XLD) measurements at the cobalt *L*-edge. We note that with out-of-plane (in-plane) linearly polarized X-rays, the cobalt *L*-edge XAS is dominated mainly by the excitation from the cobalt 2p orbitals to the unoccupied cobalt d_{xz}, d_{yz}, and $d_{3z^2-r^2}$ (d_{xy} and $d_{x^2-y^2}$) orbitals. Therefore, the different XLD spectra can provide direct information for the anisotropic electron occupation. In this study, the XLD measurements were performed with a glazing incident, as schematically shown in **Figure 4**a, in which the polarization of the X-rays was controlled between two perpendicular configurations ($E_{//}$ and $E_{\perp}$). Figure 4b shows the XLD ($IE_{//}$–$IE_{\perp}$) spectra of the LCO thin films grown at different pressures, and the negative amplitude suggests that the electrons prefer to occupy in-plane orbitals.[34–36] Upon decreasing the growth pressure, the XLD spectra are gradually suppressed, indicating that the preferred occupation is systematically weakened. To understand this evolution, we examined the origin of the XLD in Co^{3+} cations in both LS- and HS-states (Figure 4c). For LS-Co^{3+} ($t_{2g}^6e_g^0$) cations, the XLD probes mainly the e_g orbitals since the t_{2g} orbitals are fully occupied. Thus, XLD spectra origin from the lifted degeneracy of $d_{3z^2-r^2}$ and $d_{x^2-y^2}$ orbitals through tensile strain; however, its integral should be zero since these orbitals are totally empty. Similarly, for HS-Co^{3+} ($t_{2g}^4e_g^2$) cations, the XLD probes the preferred electron occupancy in both the e_g and t_{2g} orbitals, while its integral spectra are determined only by the t_{2g} orbitals since the e_g orbital is half-filled. In short, the integral of the XLD spectra provides important insights into the spin state of Co^{3+} ions through the t_{2g} orbitals. In the current system, our XLD data suggest the films grown at higher oxygen pressures show the presence of a pronounced none-zero integral XLD spectra due to sizeable concentration of HS-Co^{3+} cations, while their content decreases for samples grown at lower pressure.

We note that the spin state of Co^{3+} cations is strongly correlated with the crystal-field splitting ($\Delta_{CF} \approx 1/d^5$) and the bandwidth of the hybridized cobalt-3d orbitals with the oxygen-2p orbitals, where *d* is the bond length of Co—O.[37,38] In the current system, since the Co—O bond length (d = 1.93 Å)[5] of bulk LCO is approximately half of the in-plane lattice constant, then the bond length will not be deformed with the tensile strain. Furthermore, the elongated out-of-plane lattice constant would only lead to an increase of bond angle, but rather than a stretched bond distance as the largest out-of-plane lattice constant (3.84 Å) is still notably smaller than two times of bond length ($2d$ ≈ 3.86 Å). Therefore Δ_{CF} remains roughly constant, and we only need to consider the evolution of the bandwidth. With tensile strain, the degeneracies of both t_{2g} and e_g are lifted, resulting in an enhanced p-d hybridization as well as bandwidth. As expected, this triggers a LS-to-HS transition. While with the lattice expansion along the out-of-plane direction, the orbital degeneracy is reformed due to the reduced tetragonal distortion, which favors the LS state due to the reduced bandwidth.

To provide further insights for this phenomenological discussion, we carried out density functional theory calculations for the LCO with different lattice constants. We constructed an LCO supercell ($2 \times 2 \times 2$) with eight cobalt cations, and used the experimental lattice constants of LCO thin films grown at 20 Pa and 1 Pa. We then calculated the total energy with different combined LS and HS spin configurations (Figure S5, Supporting Information). It is important to note that for all spin configurations considered, the LCO shows a well-defined electronic bandgap, indicating robust insulating state (Figure S6, Supporting Information). The results (Figure S7, Supporting Information) show that the configurations with higher concentration of LS states are more stable in both cases, indicating the predominant role of LS Co^{3+} in LCO. Specifically, for the structure with smaller *c* lattice constant (20 Pa sample), a ferromagnetic-ordered 3:5 HS/LS configuration shows the lowest total energy, while in the sample with larger *c* (1 Pa sample), the most stable configuration transforms into ferromagnetic-ordered 1:7 HS/LS, in which both the concentration of HS Co^{3+} ions and the total magnetization are suppressed. These calculations are qualitatively consistent with our experimental results, indicating the important role of the tetragonal distortion to the emergent ferromagnetism, which is consistent with the previous studies of strained engineered LCO thin films.[24]

3. Conclusion

We have investigated the evolution of ferromagnetism as well as HS to LS transition in LCO thin films with controlled lattice degree of freedom through cation-stoichiometric engineering. The work suggests that structural deformations are the dominate factor for the emergent ferromagnetism, in which the break of orbital degeneracy due to tensile strain increasing the bandwidth and favors the HS state in Co^{3+}; while a lattice expansion due to the cobalt-cation deficiency reclaims the orbital degeneracy and consequently results in LS state in Co^{3+}. Since the cation-stoichiometry of complex oxides can be readily controlled during the growth, we envision that the current study offers a promising pathway to manipulate the electronic states of complex oxide through its imposed lattice deformation.

4. Experimental Section

Thin Film Growth: Epitaxial $LaCoO_3$ thin films were grown on (001) oriented $(LaAlO_3)_{0.3}$–$(SrAl_{0.5}Ta_{0.5}O_3)_{0.7}$ (LSAT) substrates by a custom-designed pulsed laser deposition (PLD) system using a KrF excimer laser (λ = 248 nm). During deposition, the substrate temperature was kept at 650 °C, and the oxygen pressure within the chamber was set at 20, 10, 5, and 1 Pa, respectively. The pulse frequency was 4 Hz with energy density of 1.7 J cm^{-1}. After the deposition, the samples were cooled down to room temperature at the same oxygen pressure during deposition with cooling rate of 10 °C per minute. The sample thickness was controlled by the growth time with calibrated growth rate and then confirmed with X-ray reflectometry measurements.

Structural and Compositional Analysis of Thin Films: The crystalline structures of thin films were characterized by a high-resolution four-circle X-ray diffractometer (Smartlab, Rigaku) using monochromatic Cu $K_{\alpha 1}$ radiation (λ = 1.5406 Å). The scanning transmission electron microscopy imaging and electron dispersive spectra were performed using a JOEL-ARM300F microscope with resolution up to 53 pm attached to a spherical aberration-corrector. To probe the stoichiometry of LCO thin films, the Rutherford backscattering spectrometry was taken using a Pelletron accelerator with He^{2+} energy = 2040 keV, and the fitting of experimental data was completed by RBS analysis software SIMNRA (simnra.com). To avoid the influence of La signal from the LSAT substrate, RBS measurements were carried out for LCO thin films grown on (001) oriented $SrTiO_3$ substrates with the same growth conditions as the ones grown on LSAT substrates.

Study of Magnetic and Electronic Properties: The magnetic properties including magnetic-field and temperature-dependent magnetization of thin films were measured by Quantum Design Superconducting Quantum Interference Device (SQUID). The soft X-ray absorption spectra (sXAS) including X-ray linear dichroism (XLD) and X-ray magnetic dichroism measurement of Fe *L*-edges and O *K*-edges were obtained with the luminescence yield (LY) mode at beamlines 4.0.2 and 6.3.1 of Advanced Light Source. The sXAS spectra were normalized with the photon flux measured by the photocurrent of a clean gold mesh.

Density Functional Theory Calculations: First-principles density functional theory calculations were carried out with the projector augmented wave method encoded in the Vienna Ab initio Simulation Package (VASP). The exchange-correlation functional of the Perdew–Burke–Erzerhof form was adopted and the plane-wave cutoff energy was set to 450 eV. To properly describe the strong electron correlation in the Co 3d states, the GGA plus on-site repulsion *U* method (GGA+*U*) was employed with the effective *U* value of 4.3 eV and exchange interaction J_H = 1 eV. Structure optimizations were performed for 40-atom $2 \times 2 \times 2$ supercell with $3 \times 3 \times 3$ M-P *k*-point mesh, and the atomic positions were optimized until the residual Hellman–Feynman forces were less than 0.01 eV $Å^{-1}$.

Supporting Information

Supporting Information is available from the Wiley Online Library or from the author.

Acknowledgements

T.H. and Y.L. contributed equally to this work. This study was financially supported by the National Key R&D Program of China (Grant Nos. 2021YFA1400300 and 2021YFE0107900), the Beijing Nature Science Foundation (grant No. Z200007), and the NFSC (No. 51872155, 52025024 and 92163113), S.S. acknowledges the National Science Foundation via grant DMR-2102895. L.W.M. acknowledges the Army Research Office via grant W911NF-21-1-0118. The authors acknowledge the use of facilities and instrumentation at the UC Irvine Materials Research Institute (IMRI), which is supported in part by the National Science Foundation through the UC Irvine Materials Research Science and Engineering Center (DMR-2011967).

Conflict of Interest

The authors declare no conflict of interest.

Data Availability Statement

The data that support the findings of this study are available on request from the corresponding author. The data are not publicly available due to privacy or ethical restrictions.

Keywords

cation off-stoichiometry, ferromagnetism, lanthanum cobaltate, oxygen vacancies, spin states, stain engineering

Received: November 15, 2022
Revised: January 5, 2023
Published online: March 9, 2023

[1] V. G. Bhide, D. S. Rajoria, G. R. Rao, C. N. R. Rao, *Phys. Rev. B* **1972**, *6*, 1021.
[2] T. Saitoh, T. Mizokawa, A. Fujimori, M. Abbate, Y. Takeda, M. Takano, *Phys. Rev. B* **1997**, *55*, 4257.
[3] D. P. Kozlenko, N. O. Golosova, Z. Jirák, L. S. Dubrovinsky, B. N. Savenko, M. G. Tucker, Y. L. Godec, V. P. Glazkov, *Phys. Rev. B* **2007**, *75*, 064422.
[4] G. Vankó, J.-P. Rueff, A. Mattila, Z. Németh, A. Shukla, *Phys. Rev. B* **2006**, *73*, 024424.
[5] K. Knížek, P. Novák, Z. Jirák, *Phys. Rev. B* **2005**, *71*, 054420.
[6] D. Fuchs, C. Pinta, T. Schwarz, P. Schweiss, P. Nagel, S. Schuppler, R. Schneider, M. Merz, G. Roth, H. v. Löhneysen, *Phys. Rev. B* **2007**, *75*, 144402.
[7] D. Fuchs, E. Arac, C. Pinta, S. Schuppler, R. Schneider, H. v. Löhneysen, *Phys. Rev. B* **2008**, *77*, 014434.
[8] J. M. Rondinelli, N. A. Spaldin, *Phys. Rev. B* **2009**, *79*, 054409.
[9] Y. Yokoyama, Y. Yamasaki, M. Taguchi, Y. Hirata, K. Takubo, J. Miyawaki, Y. Harada, D. Asakura, J. Fujioka, M. Nakamura, H. Daimon, M. Kawasaki, Y. Tokura, H. Wadati, *Phys. Rev. Lett.* **2018**, *120*, 206402.
[10] G. E. Sterbinsky, R. Nanguneri, J. X. Ma, J. Shi, E. Karapetrova, J. C. Woicik, H. Park, J. W. Kim, P. J. Ryan, *Phys. Rev. Lett.* **2018**, *120*, 197201.
[11] H. Hsu, P. Blaha, R. M. Wentzcovitch, *Phys. Rev. B* **2012**, *85*, 140404.
[12] H. Seo, A. Posadas, A. A. Demkov, *Phys. Rev. B* **2012**, *86*, 014430.
[13] D. Meng, H. Guo, Z. Cui, C. Ma, J. Zhao, J. Lu, H. Xu, Z. Wang, X. Hu, Z. Fu, R. Peng, J. Guo, X. Zhai, G. J. Brown, R. Knize, Y. Lu, *Proc. Natl. Acad. Sci. USA* **2018**, *115*, 2873.
[14] N. Biškup, J. Salafranca, V. Mehta, M. P. Oxley, Y. Suzuki, S. J. Pennycook, S. T. Pantelides, M. Varela, *Phys. Rev. Lett.* **2014**, *112*, 087202.
[15] V. V. Mehta, N. Biskup, C. Jenkins, E. Arenholz, M. Varela, Y. Suzuki, *Phys. Rev. B* **2015**, *91*, 144418.
[16] V. Mehta, Y. Suzuki, *J. Appl. Phys.* **2011**, *109*, 07D717.
[17] M. Merz, P. Nagel, C. Pinta, A. Samartsev, H. v. Löhneysen, M. Wissinger, S. Uebe, A. Assmann, D. Fuchs, S. Schuppler, *Phys. Rev. B* **2010**, *82*, 174416.
[18] J. Fujioka, Y. Yamasaki, H. Nakao, R. Kumai, Y. Murakami, M. Nakamura, M. Kawasaki, Y. Tokura, *Phys. Rev. Lett.* **2013**, *111*, 027206.
[19] W. S. Choi, J.-H. Kwon, H. Jeen, J. E. Hamann-Borrero, A. Radi, S. Macke, R. Sutarto, F. He, G. A. Sawatzky, V. Hinkov, M. Kim, H. N. Lee, *Nano Lett.* **2012**, *12*, 4966.
[20] J.-H. Kwon, W. S. Choi, Y.-K. Kwon, R. Jung, J.-M. Zuo, H. N. Lee, M. Kim, *Chem. Mater.* **2014**, *26*, 2496.
[21] J. Gazquez, W. Luo, M. P. Oxley, M. Prange, M. A. Torija, M. Sharma, C. Leighton, S. T. Pantelides, S. J. Pennycook, M. Varela, *Nano Lett.* **2011**, *11*, 973.
[22] E.-J. Guo, R. Desautels, D. Keavney, M. A. Roldan, B. J. Kirby, D. Lee, Z. Liao, T. Charlton, A. Herklotz, T. Z. Ward, M. R. Fitzsimmons, H. N. Lee, *Sci. Adv.* **2019**, *5*, eaav5050.
[23] U. Gebhardt, N. V. Kasper, A. Vigliante, P. Wochner, H. Dosch, F. S. Razavi, H. U. Habermeier, *Phys. Rev. Lett.* **2007**, *98*, 096101.
[24] D. Fuchs, L. Dieterle, E. Arac, R. Eder, P. Adelmann, V. Eyert, T. Kopp, R. Schneider, D. Gerthsen, H. v. Löhneysen, *Phys. Rev. B* **2009**, *79*, 024424.
[25] V. V. Mehta, M. Liberati, F. J. Wong, R. V. Chopdekar, E. Arenholz, Y. Suzuki, *J. Appl. Phys.* **2009**, *105*, 07E503.
[26] C. F. Chang, Z. Hu, H. Wu, T. Burnus, N. Hollmann, M. Benomar, T. Lorenz, A. Tanaka, H. J. Lin, H. H. Hsieh, C. T. Chen, L. H. Tjeng, *Phys. Rev. Lett.* **2009**, *102*, 116401.
[27] Q. Q. Lan, X. J. Zhang, X. Shen, H. W. Yang, H. R. Zhang, X. X. Guan, W. Wang, Y. Yao, Y. G. Wang, Y. Peng, B. G. Liu, J. R. Sun, R. C. Yu, *Phys. Rev. Mater.* **2017**, *1*, 024403.
[28] J. Chen, M. Döbeli, D. Stender, K. Conder, A. Wokaun, C. W. Schneider, T. Lippert, *Appl. Phys. Lett.* **2014**, *105*, 114104.
[29] I. Marozau, P. T. Das, M. Döbeli, J. G. Storey, M. A. Uribe-Laverde, S. Das, C. Wang, M. Rössle, C. Bernhard, *Phys. Rev. B* **2014**, *89*, 174422.
[30] T. Li, S. Deng, H. Liu, S. Sun, H. Li, S. Hu, S. Liu, X. Xing, J. Chen, *Adv. Mater.* **2021**, *33*, 2008316.
[31] D. J. Keeble, S. Wicklein, R. Dittmann, L. Ravelli, R. A. Mackie, W. Egger, *Phys. Rev. Lett.* **2010**, *105*, 226102.
[32] C. A. M. van den Bosch, A. Cavallaro, R. Moreno, G. Cibin, G. Kerherve, J. M. Caicedo, T. K. Lippert, M. Doebeli, J. Santiso, S. J. Skinner, A. Aguadero, *Adv. Mater. Interfaces* **2020**, *7*, 1901440.
[33] S. Wicklein, A. Sambri, S. Amoruso, X. Wang, R. Bruzzese, A. Koehl, R. Dittmann, *Appl. Phys. Lett.* **2012**, *101*, 131601.
[34] A. S. Disa, D. P. Kumah, A. Malashevich, H. Chen, D. A. Arena, E. D. Specht, S. Ismail-Beigi, F. J. Walker, C. H. Ahn, *Phys. Rev. Lett.* **2015**, *114*, 026801.
[35] E.-J. Guo, R. D. Desautels, D. Keavney, A. Herklotz, T. Z. Ward, M. R. Fitzsimmons, H. N. Lee, *Phys. Rev. Mater.* **2019**, *3*, 014407.
[36] Z. Liao, E. Skoropata, J. W. Freeland, E.-J. Guo, R. Desautels, X. Gao, C. Sohn, A. Rastogi, T. Z. Ward, T. Zou, T. Charlton, M. R. Fitzsimmons, H. N. Lee, *Nat. Commun.* **2019**, *10*, 589.
[37] M. Imada, A. Fujimori, Y. Tokura, *Rev. Mod. Phys.* **1998**, *70*, 1039.
[38] J. S. Zhou, J. Q. Yan, J. B. Goodenough, *Phys. Rev. B* **2005**, *71*, 220103.